

RSC Advances



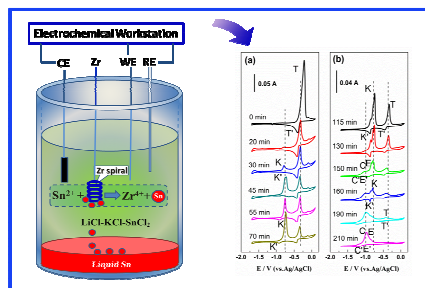
This is an *Accepted Manuscript*, which has been through the Royal Society of Chemistry peer review process and has been accepted for publication.

Accepted Manuscripts are published online shortly after acceptance, before technical editing, formatting and proof reading. Using this free service, authors can make their results available to the community, in citable form, before we publish the edited article. This *Accepted Manuscript* will be replaced by the edited, formatted and paginated article as soon as this is available.

You can find more information about *Accepted Manuscripts* in the [Information for Authors](#).

Please note that technical editing may introduce minor changes to the text and/or graphics, which may alter content. The journal's standard [Terms & Conditions](#) and the [Ethical guidelines](#) still apply. In no event shall the Royal Society of Chemistry be held responsible for any errors or omissions in this *Accepted Manuscript* or any consequences arising from the use of any information it contains.

Graphical Abstract



LiCl-KCl-ZrCl_4 melt was prepared by displacement reaction between SnCl_2 and Zr, and the reaction progress was electrochemically monitored.

Investigation of the reaction progress between stannous chloride and zirconium in molten LiCl–KCl

Cite this: DOI: 10.1039/x0xx00000x

Yanqing Cai,^a Hongxia Liu,^a Qian Xu,^{*b} Qiushi Song,^a Huijun Liu^c

Received 00th January 2012,
Accepted 00th January 2012

DOI: 10.1039/x0xx00000x

www.rsc.org/

LiCl–KCl–ZrCl₄ melt was prepared by in-situ displacement reaction between SnCl₂ and Zr in LiCl–KCl melt at 773 K, and the progress of the reaction between SnCl₂ and Zr was also investigated by dynamically electrochemical measurements, such as cyclic voltammetry, square wave voltammetry and open circuit chronopotentiometry. The results reveal that the concentration of Zr(IV) increases gradually and reaches to a maximum value with the reaction time increasing from 0 to 210 min, while the concentration of Sn(II) decreases gradually and drops below the detection limit. In addition, the chemical analyses of Zr(IV) and Sn(II) in the melt at various times were also carried out and the results are in good agreement with those of the electrochemical measurements. Finally, LiCl–KCl–ZrCl₄ melts with a low concentration of Sn(II) (<0.01 wt.%) were obtained, when the reaction time prolonged to 210 min.

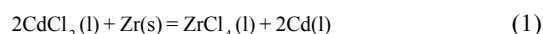
Introduction

Zirconium, as a major component, is widely used in nuclear reactors for the cladding of the nuclear fuels and the structural materials due to its low neutron-capture cross-section and high corrosion resistance under normal service conditions.¹ However, it must be nearly free of hafnium because of hafnium's large neutron capture cross-section. Hence, the refining of zirconium becomes a technology required substantially for producing the hafnium-free zirconium metal.² The electrochemical refining in the molten chlorides with ZrCl₄ has been developed as a promising option for the zirconium refining from impure zirconium metal, alloy or spent metal fuels^{3,4}.

In fact, during the electro-refining process in the molten salt, a low-melting point Cu–Sn–Zr alloy is proposed to be a liquid anode, while the highly pure zirconium can be deposited on the cathode.⁵ The method would not only reduce the operating temperature, but also provide a low cost and semi-continuous process for the production of the nuclear grade zirconium. The electrorefining of Zr should be carried out in LiCl–KCl–ZrCl₄ molten salt at the temperature higher than 773 K considering the melting point of Cu–Sn–Zr alloy as an anode. However, there is a big challenge for preparation of the molten LiCl–KCl–ZrCl₄ as an electrolyte, if ZrCl₄ is directly introduced into the salt since it is easy to be atomized due to its low boiling point of 331 °C.^{3,6,7}

Several investigators^{7–10} have attempted to prepare the molten chlorides by the oxidation of metal with CdCl₂ in the LiCl–KCl melt, and this method also can eliminate any gasification of the metal chloride with low boiling point because the chloride will preferably dissolve in the melt rather than gasify into the air.

Murakami et al.⁷ have attempted to prepare LiCl–KCl–ZrCl₄ melt by the reaction between CdCl₂ and zirconium metal according to the equation (1).



In our previous work¹⁰, we had prepared LiCl–KCl–ZrCl₄ in situ with the equilibration reaction between cuprous chloride and zirconium.

Here, considering that the liquid Cu–Sn–Zr can be used as a liquid anode, and stannous chloride is non-toxic and easily obtained, SnCl₂ was selected as the reactant for the displacement reaction with Zr in order to prepare LiCl–KCl–ZrCl₄. The liquid Sn displaced can aggregate into the liquid metal, and be removed from the molten salt. The present study focused on in-situ catching the change of electrochemical behavior of the melt with the time during the reaction between stannous chloride and zirconium in the LiCl–KCl melt by the electrochemical methods, such as cyclic voltammetry, square wave voltammetry. This dynamically electrochemical measurement and analysis could be expected for monitoring the reaction progress and determining the final of the reaction. The prepared LiCl–KCl–ZrCl₄ melt was also characterized, which will be used as the electrolyte in the electrorefining of Zr with the low-melting Cu–Sn–Zr liquid alloy anode in the future research.

Experimental

Electrochemical apparatus and chemicals

All of the electrochemical experiments were conducted under high-purity argon atmosphere. A three-electrode

electrochemical cell was assembled in an alumina crucible, which was positioned in a stainless steel vessel and heated with an electric furnace¹⁰. A graphite rod (spectrum pure) having a diameter of 14.0 mm served as the counter electrode (CE), which was provided by the Shanghai new graphite material Co., Ltd. of Sinosteel Corporation (Shanghai, China). A molybdenum wire (99.95% purity) with a diameter of 1.0 mm was used as the working electrode (WE) for the investigation of electrochemical behaviour. The active electrode surface area was determined by measuring the immersion depth of the electrode in the salt after each experiment. The reference electrode (RE) was LiCl–KCl–1.0 wt.% AgCl molten salt placed in a close-ended mullite tube with a 1.0 mm (dia.) silver wire (99.999% purity) immersed in it for electrical connections. All potentials in this work will be referred to this electrode unless otherwise stated.

A mixture of 400 g LiCl–KCl eutectic salt (59:41 mol.%) was used as the electrolyte, which was dried for more than 72 h at 573 K to remove residual water and then melted under argon atmosphere in an alumina crucible. In order to eliminate the residual water and other possible redox-active impurities, pre-electrolysis of the LiCl–KCl eutectic was conducted at 2.8 V for 2.0 h between two graphite rods prior to the electrochemical experiments. Stannous (II) ions were introduced into the bath in the form of dehydrated SnCl₂ powders. Anhydrous zirconium tetrachloride was obtained from Aladdin and used without further purification. All chemicals used in this work were of analytical grade. Molybdenum wire, silver wire, and zirconium wire were supplied by Rare Metallic Co., Ltd of Shenyang, which were used after successively polishing with sandpapers and washing with alcohol.

An AUTOLAB/PGSTAT320 potentiostat from M/s. EcoChemie, Netherlands controlled with NOVA 1.6 software for square wave voltammetry and GPES 4.9 software for cyclic voltammetry and open circuit chronopotentiometry was employed to conduct the electrochemical tests. A quantitative compositional measurement of the melt at various times was made by using an inductively coupled plasma–atomic emission spectrometer (ICP–AES). In addition, an X–ray diffractometer (XRD) was used to characterize the recovered precipitates.

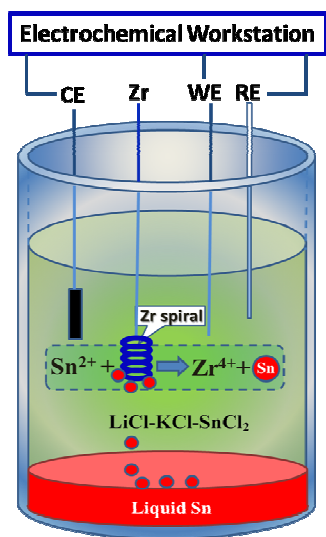


Fig. 1 Schematic diagram of the displacement reaction

Experimental procedure

After pre-electrolysis, certain amount of SnCl₂ was introduced into LiCl–KCl eutectic, and then a zirconium spiral (99.4% purity) more than the stoichiometric amount was introduced when the salt was in a stable condition. Then displacement reaction between zirconium and SnCl₂ occurred. The schematic diagram of the displacement reaction process is shown in Fig. 1. Zr(IV) ions were generated and entered the molten salt during the displacement reaction, and tin was produced in the form of droplets because of the low-melting point and then deposited at the bottom of the crucible. During the reaction process, the electrochemical behaviour of Zr(IV) and Sn(II) were investigated to monitor the reaction progress by cyclic voltammetry, square wave voltammetry and open circuit chronopotentiometry at various times. Cyclic voltammetry was carried out by changing the applied potential as a scan rate of 100 mV·s⁻¹, and the objective was to determine the redox peak potentials of zirconium and tin in LiCl–KCl melt. Meanwhile, the melt was sucked out at various times by a quartz tube during the reaction process, and the concentrations of tin and zirconium in the melt were determined by the ICP–AES analysis.

Results and discussion,

Cyclic voltammograms for LiCl–KCl melt, LiCl–KCl–SnCl₂ melt and LiCl–KCl–ZrCl₄ melt

A group of typical cyclic voltammograms (CVs) recorded at a molybdenum working electrode are exhibited in Fig.2, which are performed in LiCl–KCl melt (curve 1) and the melt with the addition of 0.36 wt.% SnCl₂ (curve 2) and 0.25 wt.% ZrCl₄ (curve 3), respectively. The purpose is to determine the redox peak potentials of zirconium and tin in LiCl–KCl melt, which will provide the basal potentials for the determination of zirconium and tin redox peaks in the displacement reaction process. The cathodic peak A' at –2.50 V vs. Ag/AgCl and the corresponding anodic peak A are observed as shown in curve 1, which correspond to the deposition and dissolution of metal Li¹¹. In the CV of LiCl–KCl–0.36 wt.% SnCl₂ melt as shown in curve 2, the small cathodic peak T' at around –0.50 V is attributed to the reduction of Sn²⁺ to metallic Sn. Then the corresponding anodic peak observed at –0.30 V is related to the oxidation of Sn to Sn(II)^{12, 13}. What's more, another three couples G₁/G₁', G₂/G₂' and G₃/G₃' are observed at potentials between –2.0 and –2.5 V, which should be attributed to the formation and dissolution of Sn–Li intermetallic compounds¹⁴. The results are in good agreement with the Sn–Li phase diagram¹⁵, which has four intermetallic compounds, i.e., Li₅Sn₂, Li₁₃Sn₅, Li₇Sn₂, and Li₂₂Sn₅. Among them, the first two are probably too close in composition that they could not be distinguished by means of cyclic voltammetry.

In the CV of LiCl–KCl–0.25 wt.% ZrCl₄ melt, several new peaks appear compared to the CV of LiCl–KCl melt (curve 1) as shown in curve 3. According to the references reported by several investigators^{3, 6, 16–18}, the two cathodic peaks E' and C' at around –1.15 and –1.22 V are related to the multi-step reduction of zirconium, which are corresponding to the reactions given in equations (2), (3) and (4). What's more, Sakamura¹⁷ has also reported another peak D' at –1.65 V in LiCl–KCl melt containing 1.07 wt.% ZrCl₄, which corresponds to the reduction of ZrCl to Zr. Correspondingly, another reaction related to the reduction of Zr(IV) to ZrCl is also observed at peak C'. It might be explained by the reduction mechanism of Zr(IV). Competitive reactions between the reduction of Zr(IV) to ZrCl and Zr(IV) to Zr exist during the reduction of Zr(IV). At high concentrations of Zr(IV), Peak C' is attributed to the reduction of Zr(IV) to ZrCl and Zr simultaneously.

However, at low Zr(IV) concentrations, Zr(IV) would only reduce to Zr¹⁷. Therefore, in the present work, Zr(IV) concentration is so low (0.25 wt.%) that the reduction peak of Zr(IV) to ZrCl at peak C' and the following reduction peak of ZrCl to Zr are not observed.

For the oxidation process, the corresponding anodic peaks C and E are found at around -0.95 and -0.88 V, which relate to the oxidation of Zr to Zr(II) and Zr(IV), and Zr(II) to Zr(IV), respectively, as shown in equations (5) ~ (7). Among them, peak E is not very clear and always masked by peak C³.

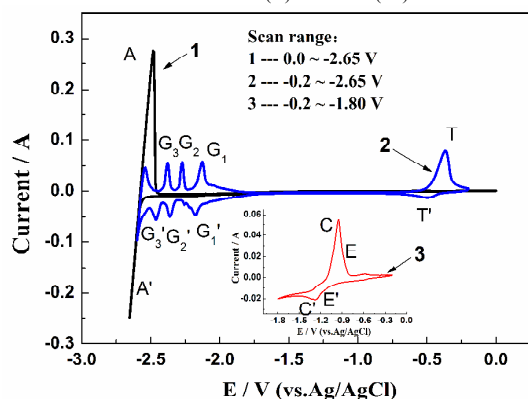
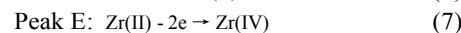
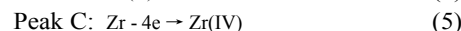
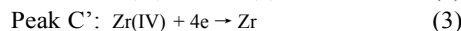
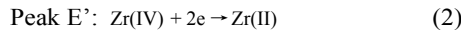


Fig. 2 CVs of blank LiCl-KCl melt (curve 1), LiCl-KCl-0.36 wt.% SnCl₂ melt (curve 2) and LiCl-KCl-0.25 wt.% ZrCl₄ (curve 3, the inset) on molybdenum electrode at 773 K. Apparent electrode area: 0.628 cm², scan rate: 100 mV·s⁻¹.

Due to low concentration and diffusion rate of the cations, e.g., Zr⁴⁺ and Sn²⁺, the reductions are controlled by the diffusion process and the rates are relatively slow, leading to small reduction peaks, such as T', E' and C'. However, the reductions continue when the potential keeps on sweeping to the negative direction, with more reductants depositing. Subsequently, the oxidation rates of the deposited tin and zirconium are relatively high, which are controlled by the electrochemical process, and the corresponding anodic peaks are prominent³.

Displacement reaction process

The reaction between SnCl₂ and Zr started when an excess of Zr was added into LiCl-KCl eutectic salt with 0.57 wt.% SnCl₂. The reaction process was monitored by in-situ recording CVs, as shown in Fig. 3. It is obvious that the electrochemical behaviours of tin and zirconium are changed with the progress of the reaction, which would be analysed in detail below.

Redox behavior of tin. As shown in Fig. 3(a, 0 min), a large cathodic peak T' at -0.50 V and a high anodic peak T at around -0.30 V are observed in LiCl-KCl-0.57 wt.% SnCl₂ melt before the introduction of zirconium, which are attributed to Sn²⁺/Sn redox couple according to Fig. 2 (curve 2).

After the introduction of zirconium spiral, a declining trend of the redox peaks of Sn²⁺/Sn couple is observed, as shown in Fig. 3(0 ~ 210 min). The result proves that the reaction between SnCl₂ and Zr goes smoothly according to equation (8), which is thermodynamically favorable according to the very high value of equilibrium constant¹⁹.

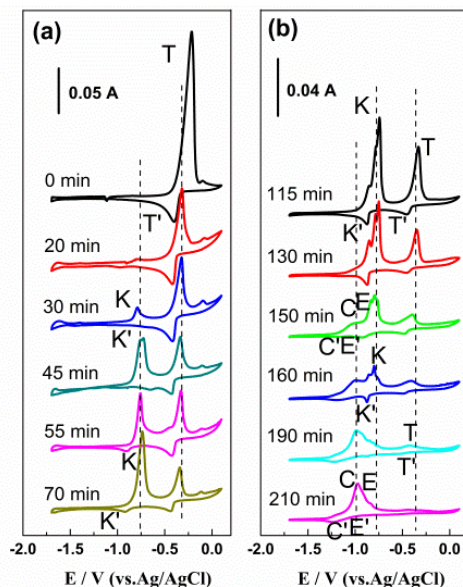
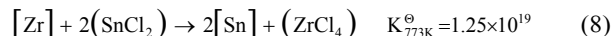


Fig. 3 CVs of LiCl-KCl-0.57 wt.% SnCl₂ melt with excessive Zr spiral at various times during the displacement reaction on molybdenum electrode at 773 K. Apparent electrode area: 0.628 cm², scan rate: 100 mV·s⁻¹.

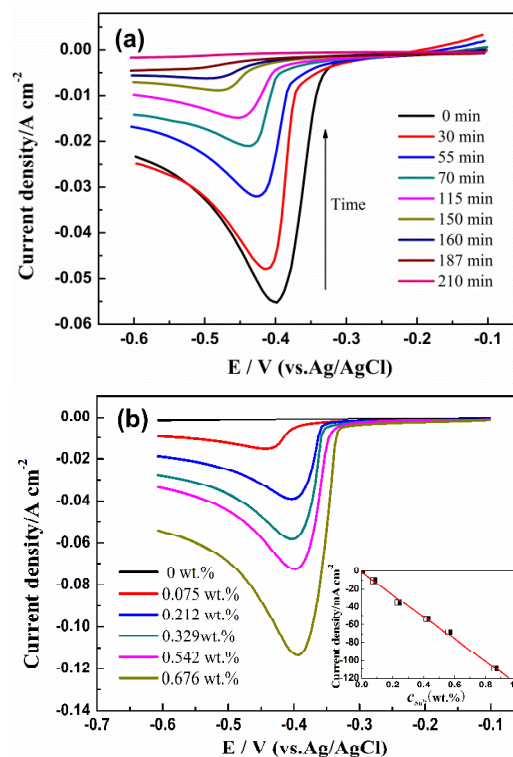


Fig. 4 (a) High-resolution CVs of the cathodic peak T' in Fig. 3, and (b) CVs of LiCl-KCl-SnCl₂ melt at various Sn(II) concentrations on molybdenum electrode at 773 K, the inset shows the relationship between the peak current I_{pc} and $c_0(\text{Sn(II)})$. Scan rate: 100 mV·s⁻¹.

It is very important to detect the Sn(II) concentration because it can reveal the reaction progress. In addition, as an impurity of

the final LiCl–KCl–ZrCl₄ melt, the final Sn(II) concentration should be strictly controlled. To obtain more details about the Sn(II) concentration, the high-resolution CVs of cathodic peak T' at different times in Fig. 3 are presented in Fig. 4(a). Apparently, a declining trend about the cathodic peak currents is observed. To further explore the relationship between Sn(II) concentration and peak current, the variation of the cathodic peak T' at various Sn(II) concentrations (c_0) was also studied and shown in Fig. 4(b). A linear relationship between the peak current I_{pc} and c_0 is obtained and shown in the inset of Fig. 4(b), according to the Berzins–Delahay equation as shown in equation (9)²⁰. The calculated Sn(II) concentrations at various times in Fig. 4(a) are exhibited in Table 1 according to equation (9).

$$I_{pc} = -0.157c_0 \quad (9)$$

Table 1 The calculated and measured data of Sn(II) concentration at various times

Time / min	$I_p / \text{A cm}^{-2}$	$c_{\text{cal}} / \text{wt.}\%$	$c_{\text{ICP}} / \text{wt.}\%$
0	-0.0553	0.352	0.356
30	-0.0479	0.305	0.285
55	-0.0320	0.204	0.199
70	-0.0211	0.134	0.128
115	-0.0148	0.094	0.092
150	-0.0089	0.067	0.068
160	-0.0062	0.039	0.037
190	-0.0040	0.025	0.023
210	-0.0010	0.006	< 0.01

For verifying the accuracy of the calculated results, Sn(II) concentration was also determined by ICP–AES analysis, as shown in Table 1. By comparison, good agreement is found between the measured and calculated data under all conditions examined, implying that equation (9) can be used for assuming the concentration of Sn(II) and monitoring the reaction progress. Additionally, it shows that the reaction has fully completed in 210 min.

Redox behavior of Zr and Sn–Zr intermetallic compounds. New redox couples K/K', C/C' and E/E' are observed at potentials between -0.75 and -1.50 V with the introduction of zirconium, as shown in Fig. 3. Their appearance suggests that Zr(IV) was produced during the reaction between zirconium and SnCl₂. From 30 to 160 min, the couple K/K' is observed at potentials between -0.75 and -1.15 V. Since the peak potentials of K/K' in Fig. 3 are more positive than that of zirconium, they are deduced to be the redox peaks of Sn–Zr intermetallic compounds. This could be explained by the so-called “underpotential deposition”^{21–23}, the deposition of Zr on the previously deposited Sn surface could electrochemically occur at a more positive potential compared to that on the pure Zr metal. It is similar to the underpotential deposition of Zr on the Sn cathode, with the formation of Sn–Zr intermetallic compounds. According to the Sn–Zr phase diagram¹⁹, three intermetallic compounds are available, i.e. SnZr, Sn₃Zr₅ and SnZr₄. However, in the present study, their potentials are probably too close and they could not be distinguished by means of cyclic voltammetry. Then the couple K/K' are used to represent all of them in the following discussion.

The peaks for the couple K/K' appear after the displacement reaction last for 30 min and then increase to the maximum value until 115 min, and finally decrease and disappear. The reason is that the formation of these intermetallic compounds firstly increases and then declines with the passage of reaction time, as the concentration of

Sn(II) decreases and Zr(IV) increases. Meanwhile, the peaks for couples C/C' and E/E' appear and increase gradually when the reaction time reaches to 150 min, which are corresponding to the couples Zr(IV)/Zr(II), and Zr(II)/Zr and Zr(IV)/Zr, respectively, according to Fig. 2. It indicates that apart from the formation of Sn–Zr intermetallic compounds, the reduction and oxidation of zirconium occur when the Zr(IV) ions are excessive in the melt. Finally, the peak currents of C/C' and E/E' increase continuously and go to the maximum value while T/T' and K/K' disappear, which suggests the completion of the reaction.

CV was performed when the displacement reaction time reached 210 min, as shown in Fig. 3(b, 210 min), and the peaks for couples C/C' and E/E' are both observed. All peaks are consistent with the behaviour of zirconium in Fig. 2 (curve 3), which is measured by the directly introducing of the ZrCl₄, implying that the generated Zr ions in the melt are in the form of Zr(IV). Additionally, no current peaks corresponding to Sn are observed, suggesting that all the Sn(II) ions have been reduced to metallic form within 210 min and only Zr(IV) remains in the melt.

Square wave voltammetry

To further confirm the cathodic peaks K', C' and E', square wave voltammetry, a method more sensitive than the conventional cyclic voltammetry, was carried out to further monitor the displacement reaction progress in-situ^{23–25}.

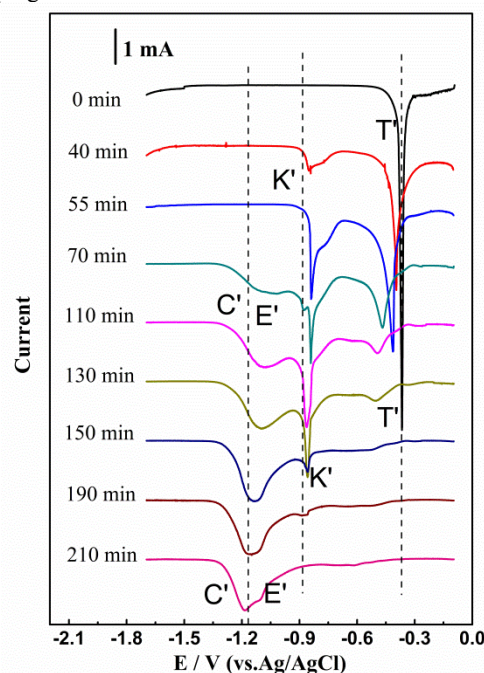


Fig. 5 SWVs of LiCl–KCl–0.57 wt.% SnCl₂ melt with excessive Zr spiral at various times during the displacement reaction on molybdenum electrode at 773 K. Apparent electrode area: 0.628 cm², frequency: 20 Hz, pulse height: 15 mV, potential step: 1 mV.

Fig. 5 shows a series of square wave voltammograms (SWVs) detected at different times during the reaction between SnCl₂ and Zr in LiCl–KCl–0.57 wt.% SnCl₂ melt at a step potential of 1 mV and frequency of 15 Hz. Before the introduction of zirconium (0 min), a large cathodic signal (peak T') is observed at -0.45 V, which is associated with the reduction of Sn(II) to metallic Sn. After the introduction of zirconium (40 ~ 210 min), the peak currents of T'

decrease gradually with the peak potential shifting negatively, indicating that the Sn(II) concentration declines with the progress of reaction. What's more, a new reduction peak K', corresponding to the Sn-Zr intermetallic compounds obtained at -0.95 V, is observed from 40 to 190 min. The peak current of K' firstly increases and then decreases, and finally disappears from the curves. Simultaneously, when the reaction time prolongs to 70 min, peaks of C' and E' appear, which are attributed to the multi-step reduction of zirconium. It indicates that there is excess Zr(IV) remaining in the melt after the formation of Sn-Zr intermetallics. From 70 to 210 min, peak currents of C' and E' increase gradually, which suggests the increase of the Zr(IV) concentrations in the melt. Finally, only peaks C' and E' remain until 210 min, and peaks T' and K' have completely disappeared. It implies that the reaction is completed, and Sn(II) ions are exhausted while only Zr(IV) ions remain. The results of square wave voltammetry are in excellent agreement with those obtained from the CV measurements.

Open circuit chronopotentiometry

In order to further investigate the progress of displacement reaction, open circuit chronopotentiometry was performed for observing the formation and dissolution of metals and intermetallic compounds. During the reaction process, a thin layer of alloy was firstly prepared by cathodic deposition on the molybdenum electrode for a period of 10 s at -2.60 V. Then the open-circuit potential of the electrode was registered as a function of time after switching off the potentiostatic control. After that, the potential plateaus equal to biphasic equilibrium of coexisting states at the electrode surface would be observed^{21, 23}.

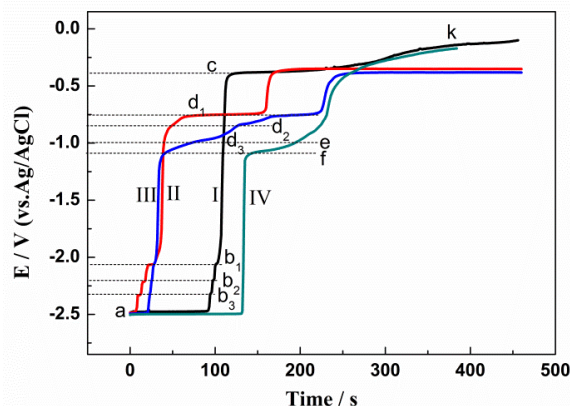


Fig. 6 OCPs of LiCl-KCl-0.57 wt. % SnCl₂ melt after electrodepositing at -2.60 V vs. Ag/AgCl for 10 s on molybdenum electrode at 773 K. (I) before the introduction of Zr spiral, 0 min, (II) after the introduction of excessive Zr spiral for 60 min, (III) 140 min and (IV) 210 min. Apparent electrode area: 0.628 cm².

Fig. 6 illustrates a set of open circuit chronopotentiograms (OCPs) obtained at different periods during displacement reaction. Curve (I) provides an OCP measured in LiCl-KCl-0.57 wt.% SnCl₂ melt before the introduction of Zr. In the beginning, a stable potential at around -2.50 V (plateau a) is observed, which refers to the Li⁺/Li equilibrium potential. Afterwards, three new plateaus b₁, b₂, b₃ at -2.05 , -2.20 , and -2.32 V are obtained respectively, which are related to the dissolution of Sn-Li intermetallic compounds. Finally, plateau c located at -0.38 V appears, which is associated with the equilibrium potential of Sn²⁺/Sn redox couple. What's more, plateau k at -0.2 V should be associated with the open circuit potential of molybdenum electrode. Curve (II) shows an OCP obtained after the reaction reaches 60 min. Apart from the plateaus observed in curve (I), a new plateau d₁ is observed at -0.75 V, which should

correspond to one of the Sn-Zr intermetallic compounds. With the reaction reaching 140 min, new plateaus d₂, d₃, e and f are observed in the potential range from -0.85 to -1.10 V in curve (III), respectively. Similarly, plateaus d₂ and d₃ should be correlated with the formation of the other two Sn-Zr intermetallic compounds. Additionally, plateau f should be associated with the deposited Zr corresponding to the equilibrium potential of Zr(IV)/Zr and Zr(II)/Zr redox couples, and plateau e might correspond to Zr(IV)/Zr(II) couple, which is coincident with the signal of Sn-Zr intermetallic compound (plateau d₃). When the displacement reaction is over, the OCP obtained at 210 min is shown in curve (IV). It is obvious that plateau f becomes more defined than that in curve (III), which can be deduced that more metallic Zr has been deposited on the electrode surface with the increasing reaction time. It is rather remarkable that plateaus c, d₁ and d₂ disappear from curve (IV), which indicates the absence of Sn(II) ions. Moreover, the plateau at -1.0 V should only correspond to Zr(IV)/Zr(II) couple (plateau e) at this time. Apparently, the results obtained by the open circuit chronopotentiometry test are well consistent with those observed in the CVs and SWVs.

Characterization of the melt and byproducts

To further investigate the progress of the reaction, the concentrations of tin and zirconium in the melt were determined by the ICP-AES analysis at various times. Fig. 7 exhibits the variation of Sn and Zr concentrations with reaction time in LiCl-KCl melt containing 1.14 wt. % SnCl₂. The concentration of Sn decreases gradually while the concentration of Zr increases as the reaction prolongs. What's more, the reaction rate in the beginning (0 ~70 min) is higher than later (70 ~ 210 min). This may be because the concentrations of the reactants (SnCl₂, Zr) in the initial stage are high, then the reaction is fast. In the second stage, the concentration of Sn(II) decreases continuously and drops to below the detection limit of the ICP-AES analysis with the reaction time prolonging to 210 min. The concentration of Zr increases to the maximum value, indicating that almost all of Sn(II) has reacted with Zr metal and the reaction is completely finished within 210 min. The ICP-AES analysis results are well consistent with the electrochemical measurement results.

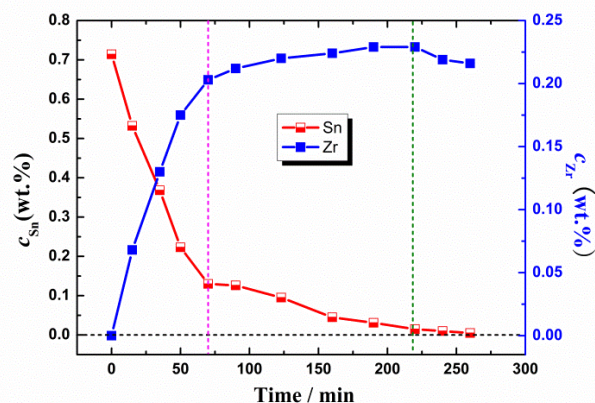
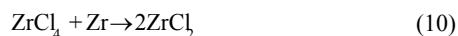


Fig.7 The effect of reaction time on concentration of Sn and Zr dissolved in LiCl-KCl-1.14 wt. % SnCl₂ melt.

However, with the reaction continuing, there is a slight decline with the concentration of Zr(IV). The slight decline of Zr(IV) may be explained from two aspects. On the one hand, it may be explained by the equation (10). Zr(IV) is attacked by excessive Zr and forming Zr(II), which might have a low solubility in the melt. In addition, Basile¹⁶ and Sakamura¹⁸ have also investigated the corrosion of Zr with ZrCl₄, and the former insisted that Zr(II) chloride is insoluble. Both of them agree that the ZrCl₂ generated in equation (10) is

unstable and would disproportionate to $ZrCl_4$ and metallic Zr powders, according to equation (11). In the authors' review, the reactions (10) and (11) might be approximately reversible, and Zr(II) might have a low solubility in the melt, leading the decline of Zr(IV). On the other hand, the soluble Zr(IV) and partly soluble Zr(II) chlorides easily reacted with oxygen, which may be introduced by the moisture in the flowing argon, resulting in the formation of insoluble ZrO_2 and the final decrease of the zirconium concentration in the melt¹. In a word, the final zirconium content remains nearly constant and the measured CV does not change in shape after a long time contact between Zr and Zr(IV), indicating that the existence of Zr(II) in the melt may do not have any influence¹⁸. Finally, almost all the zirconium ions remained in the melt are in the form of Zr(IV).



To further confirm the final concentration of Zr(IV), a series of displacement experiments with different initial $SnCl_2$ concentrations and excess Zr were conducted. And the masses of Zr, before and after the displacement experiment and dissolved in the melt were measured. Table 2 shows the comparison of the calculated weight losses of zirconium (m_1^a) and experimental weight losses of zirconium (m_2^b), and the final masses of zirconium dissolved in the melt (m_3^c) with different initial $SnCl_2$ concentrations.

Among them, test No.1 is corresponding to the electrochemical tests in Section 3.1.2, 3.2, 3.3 and test No.2 is corresponding to the ICP-AES analysis in Fig. 7. By comparison, the experimental weight losses of zirconium are higher than the calculated data by equation (8), while the dissolved masses of zirconium are lower than them. Combing with the above interpretations, the possible reason is that there are two kinds of contributions to the weight losses of zirconium. One is due to the participation in the displacement reaction, and the other is the participation in the reaction shown in equation (10). This results in the increase of the experimental weight losses and the decrease of the dissolved zirconium masses. However, due to the equilibrium between the equation (10) and (11), the dissolved zirconium is slightly less than the calculated value. Finally, the LiCl-KCl-ZrCl₄ melts are obtained with relatively stable concentrations of ZrCl₄ (0.28 wt.% ~1.17 wt.%).

Table 2 Calculated and experimental weight losses of zirconium and the weight of zirconium dissolved in melt

Test No.	Initial concentration of $SnCl_2$ (wt.%)	m_1^a/g	m_2^b/g	m_3^c/g	Final concentration of $ZrCl_4$ (wt.%)
1	0.57	0.55	0.94	0.43	0.28
2	1.14	1.10	2.68	0.89	0.57
3	2.09	2.01	2.91	1.83	1.17

^a m_1Calculated weight loss of zirconium

^b m_2Experimental weight loss of zirconium

^c m_3Mass of zirconium dissolved in melt

The tin and zirconium precipitates were obtained and characterized as shown in Fig. 8. A clear layer structure with dark grey precipitates at the bottom and the molten salt in the upper layer are observed according to their different densities. After washing with water, the precipitates are determined as a mixture of Sn, $ZrSn_2$, $ZrSn$, ZrO_2 and Zr by the XRD analysis as shown in Fig.8(b). Undoubtedly, metallic Sn is obtained by the displacement reaction, while zirconium powders are caused by the disproportionation reaction of

$ZrCl_2$. Then $ZrSn_2$ and $ZrSn$ are formed spontaneously with low formation energies. ZrO_2 is obtained due to the oxidation of metallic zirconium powders during the washing and drying process, as they are easily oxidized even at low temperatures in accordance with the calculation by the HSC code³, as well as by the oxidation and hydroxylation of zirconium chlorides. Its formation can be avoided in the continuous operation. In the actual refining experiment, the recovered copper and zirconium would be returned to the liquid Cu-Sn-Zr alloy at the bottom of the crucible for reusing continuously in the electrorefining process.

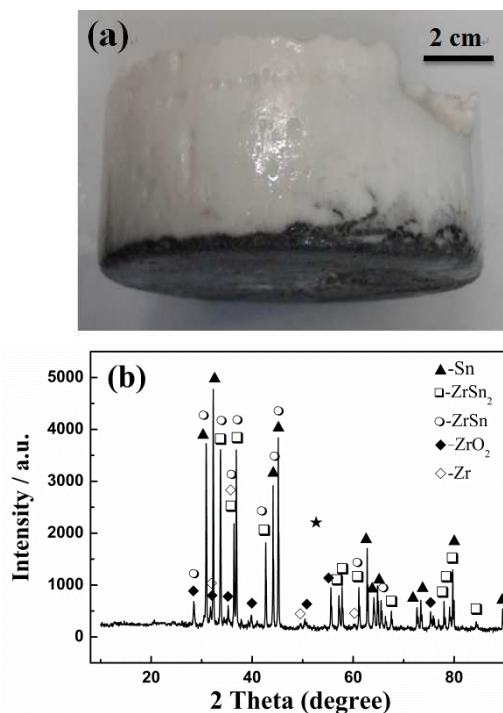


Fig.8 (a) Photo of the melt and products, and (b) XRD pattern of the products at the bottom of the crucible.

Conclusions

The in-situ preparation of LiCl-KCl-ZrCl₄ melt by the displacement reaction between Zr and $SnCl_2$ was investigated in LiCl-KCl molten salt at 773 K, and the reaction progress was also monitored in-situ by a series of electrochemical methods, such as cyclic voltammetry, square wave voltammetry and open circuit chronopotentiometry. The electrochemical results reveal that the concentration of Zr(IV) gradually increases with the decline of Sn(II) concentration and reaches to the maximum value, while Sn(II) drops to below the detection limit when the reaction time prolongs to 210 min. The chemical analyses of Zr(IV) and Sn(II) are in good agreement with the electrochemical results. As a result, the reaction progress between $SnCl_2$ and zirconium is clearly presented, and LiCl-KCl-ZrCl₄ melts with low concentration of Sn(II) (<0.01 wt.%) are obtained, which is proposed to be used as electrolyte in the electrorefining of Zr with the low-melting Cu-Sn-Zr liquid alloy anode in the future.

Acknowledgements

The authors acknowledge the financial support of National Natural Science Foundation of China (Grant No. 51174055).

Notes and references

a School of Materials Science and Metallurgy, Northeastern University, Shenyang, 110004, PR China

b School of Materials Science and Engineering, Shanghai University, Shanghai, 200072, PR China

c Laboratory for Corrosion and Protection, Institute of Metal Research, Chinese Academy of Sciences, Shenyang, 110016, PR China

1. D. L. Douglass, *Metallurgy of zirconium*, Univ. of California, Los Angeles, 1971.
2. W. J. Kroll and F. E. Bacon, US Patent, 443,253, 1948.
3. C. H. Lee, K. H. Kang, M. K. Jeon, C. M. Heo and Y. L. Lee, *J. Electrochem. Soc.*, 2012, **159**, D463.
4. K. T. Park, T. H. Lee, N. C. Jo, H. H. Nersisyan, B. S. Chun, H. H. Lee and J. H. Lee, *J. Nucl. Mater.*, 2013, **436**, 130.
5. Y. Xiao, A. V. Sandwijk, Y. Yang and V. Laging, *Molten Salts Chem. Tech.*, 2014, 389.
6. J. Park, S. Choi, S. Sohn, K. Kim and I. S. Hwang, *J. Electrochem. Soc.*, 2014, **161**, H97.
7. T. Murakami and T. Kato, *J. Electrochem. Soc.*, 2008, 155, E90-E95.
8. S. Kuznetsov, H. Hayashi, K. Minato and M. Gaune-Escard, *J. Electrochem. Soc.*, 2005, **152**, C203.
9. S. Ghosh, S. Vandarkuzhali, N. Gogoi, P. Venkatesh, G. Seenivasan, B. P. Reddy and K. Nagarajan, *Electrochim. Acta*, 2011, **56**, 8204.
10. Y.Q. Cai, H.X. Liu, Q. Xu, Q.S. Song, L. Xu, *Electrochim. Acta*, 2015, **161**, 177.
11. H. Tang, Y. D. Yan, M. L. Zhang, X. Li, Y. Huang, Y. L. Xu, Y. Xue, W. Han and Z. J. Zhang, *Electrochim. Acta*, 2013, **88**, 457.
12. H. El Ghallali, H. Groult, A. Barhoun, K. Draoui, D. Krulic and F. Lantelme, *Electrochim. Acta*, 2009, **54**, 3152.
13. H. Groult, H. El Ghallali, A. Barhoun, E. Briot, L. Perrigaud, S. Hernandez and F. Lantelme, *Electrochim. Acta*, 2010, **55**, 1926.
14. Q. Xu, C. Schwandt and D. J. Fray, *J. Electroanal. Chem.*, 2004, **562**, 15.
15. W. G. Moffatt, *The handbook of binary phase diagrams*, Genium Pub. Corp., 1976.
16. F. Basile, E. Chassaing and G. Lorthioir, *J. Appl. Electrochem.*, 1981, **11**, 645.
17. S. Ghosh, S. Vandarkuzhali, P. Venkatesh, G. Seenivasan, T. Subramanian, B. Prabhakara Reddy and K. Nagarajan, *J. Electroanal. Chem.*, 2009, **627**, 15.
18. Y. Sakamura, *J. Electrochem. Soc.*, 2004, **151**, C187.
19. I. Barin, *Thermochemical data of pure substances*, Wiley-VCH Verlag GmbH, Weinheim, 1995.
20. A. J. Bard and L. R. Faulkner, *Electrochemical methods: fundamentals and applications*, Wiley New York, 1980.
21. X. Li, Y.D. Yan, M.L. Zhang, Y. Xue, H. Tang, D.B. Ji and Z.J. Zhang, *RSC Adv.*, 2014, **4**, 40352.
22. W. Xiao and D. Wang, *Chem. Soc. Rev.*, 2014, **43**, 3215.
23. Y.L. Liu, Y.D. Yan, W. Han, M.L. Zhang, L.Y. Yuan, K. Liu, G.-A. Ye, H. He, Z.-F. Chai and W.Q. Shi, *RSC Adv.*, 2013, **3**, 23539.
24. L. Wang, Y.L. Liu, K. Liu, S.L. Tang, L.Y. Yuan, L.L. Su, Z.F. Chai and W.Q. Shi, *Electrochim. Acta*, 2014, **147**, 385.
25. Y. Liu, Y. Yan, W. Han, M. Zhang, L. Yuan, R. Lin, G. Ye, H. He, Z. Chai and W. Shi, *Electrochim. Acta*, 2013, **114**, 180.